

Breathing mode in an improved transport approach

T. Gaitanos¹, A.B. Larionov^{1,2}, H. Lenske¹, U. Mosel¹

¹*Institut für Theoretische Physik, Justus-Liebig-*

Universität Giessen, D-35392 Giessen, Germany

²*Russian Research Center Kurchatov Institute, RU-123182 Moscow, Russia*

(Dated: January 17, 2021)

Abstract

The nuclear breathing-mode giant monopole resonance is studied within an improved relativistic Boltzmann-Uehling-Uhlenbeck (BUU) transport approach. As a new feature, the numerical treatment of ground state nuclei and their phase-space evolution is realized with the same semiclassical energy density functional. With this new method a very good stability of ground state nuclei in BUU simulations is achieved. This is important in extracting clear breathing-mode signals for the excitation energy and, in particular, for the lifetime from transport theoretical studies including mean-field and collisional effects.

PACS numbers: 21.65.-f, 21.60.-n, 24.30.Cz, 21.60.Ev

I. INTRODUCTION

A giant monopole resonance (GMR), i.e. a collective isoscalar 0^+ excitation of a nucleus, has been extensively investigated in the past few decades, both theoretically and experimentally (see Ref. [1] for the most recent review). It is nowadays well established, that the GMR is a nuclear compression mode governed mostly by the incompressibility modulus K_∞ of nuclear matter [2], which is the key quantity for the description of nuclei, supernovae explosions, neutron stars, and heavy-ion collisions.

Many microscopic models have been developed for the theoretical description of giant resonances. They can be divided into two groups: purely quantum mechanical approaches and semi-classical dynamical models.

The former group includes the models based on the nonrelativistic [3, 4] or relativistic [5, 6] static Hartree-Fock plus random phase approximation (RPA) method. The RPA technique can be derived from a more general time-dependent Hartree-Fock (TDHF) theory (c.f. [7, 8]) in the case of small-amplitude excitations. The damping of a collective mode in a pure mean field RPA picture originates from the coupling to the particle-hole excitations (Landau damping or fragmentation width) and from coupling to the continuum states, which is equivalent to the particle loss in TDHF calculations [7]. Also constrained relativistic mean-field approaches have been developed and applied in the case of a GMR [8–10]. The collective nature of the GMR in these quantum mechanical prescriptions manifests itself from a coherent superposition of many single-particle transitions from one major shell to another [11]. Generally, within uncertainties of an underlying energy-density functional, the fully quantum approaches are able to describe the GMR energies for various sets of nuclei. However, the conclusions of different authors on the GMR total width are clearly different. Sagawa et al. [4] claim that the Landau damping and coupling to the continuum states explain the major part of the total GMR width for the ^{208}Pb nucleus and Sn isotopes. However, Piekarewicz and Centelles [6] state that the RPA calculation fails to account for the spreading component of the full escape-plus-spreading width because of the lack of coupling to the more complex than particle-hole configurations.

The second group of models [12]–[21] solves the BUU(-like) or Vlasov(-like) equations, which are the semiclassical limits of a quantum kinetic equation [22]. An advantage of the kinetic transport equation with respect to the TDHF theory is that binary collisions are

naturally included, apart the interaction between the particles due to the classical nuclear mean-field. In the classical picture, a GMR can be qualitatively understood in terms of a radial collective vibration of a nucleus: protons and neutrons oscillate in phase with a certain amplitude, which is damped due to dissipation. For this reason, the GMR is often referred to as a "breathing mode". The frequency of the breathing mode characterizes the excitation energy and the temporal damping of the amplitude — the life time of the resonance.

Semi-classical treatments of a GMR in finite nuclei have been so far restricted to pure Vlasov dynamics [18, 20, 21], where any collisional effects are completely neglected. Thus, these models predicted the excitation energy of the breathing mode appropriate well, but not the width. Alternatively, the collisional effects in the semi-classical description of the GMR were modeled within a linearized Landau-Vlasov equation [17], which, however, takes into account the finite size effects only very approximately. There are several works where the Boltzmann-Nordheim-Vlasov approach – which takes into account the selfconsistent nucleon mean field and nucleon-nucleon collisions – has been applied to the collective dipole [23, 24] and quadrupole [25] motions excited in heavy-ion collisions at low energies.

The present work is an attempt to describe simultaneously the centroid energy and the width of a GMR in finite nuclei. To this aim, we perform the full BUU calculations taking into account both the mean field and collision term. The results of the full BUU calculations are then compared with the results of solution of the Vlasov equation to make the quantitative conclusions on the contribution of two-body collisions to the total GMR width.

The numerical solution of a BUU equation for the case of a small-amplitude collective vibration excited in a finite nuclear system is extremely difficult. It requires a very good stability of the ground state configurations, which is difficult to reach in a test-particle technique underlying any numerical method to solve the BUU equation. So far empirical density distributions have been used to initialize ground state nuclei in transport theoretical simulations, which might be not always consistent with the energy density functional used for the propagation of the system. Another well known problem (see e.g. discussions in Refs. [12–14]) is related to the calculation of Pauli blocking factors in the Uehling-Uhlenbeck collision integral for the small-amplitude Fermi surface distortions.

We thus have improved the relativistic transport approach [26–28] based on the Giessen Boltzmann-Uehling-Uhlenbeck (GiBUU) transport model [29] by performing relativistic Thomas-Fermi (RTF) calculations with the same energy-density functional as that used

in the dynamical evolution. In this context, the isovector-vector ρ meson field together with its gradient terms have been included in the calculations of the present work. The initialization of neutron and proton densities according to the RTF calculation largely improves the ground-state stability in numerical simulations of the Vlasov and BUU dynamics. We have also worked out to improve the numerical treatment of the Pauli blocking in test-particle simulations of the small-amplitude nuclear motions, in-particular, in the nuclear surface regions.

The structure of the work is as follows: the standard theoretical background is presented in section II. The modified initialization procedure and numerical treatment of the Pauli blocking are then presented in section III. In section IV, results of the ground state simulations are discussed, before the calculations of the GMR excitations are presented. Finally, conclusions and outlook are presented in the last section V.

II. THE RELATIVISTIC TRANSPORT EQUATION

The baryonic mean-field is modeled within the non-linear Walecka model (mean-field approximation of the QHD) [30, 31]. The non-linear Walecka model Lagrangian includes the nucleon field ψ , the isoscalar-scalar σ meson field, isoscalar-vector ω meson field, isovector-vector $\vec{\rho}$ meson field and the electromagnetic field \mathcal{A} and reads ($\hbar = c = 1$) as:

$$\begin{aligned} \mathcal{L} = & \bar{\psi}[\gamma_\mu(i\partial^\mu - g_\omega\omega^\mu - g_\rho\vec{\tau}\vec{\rho}^\mu - e\frac{1+\tau_3}{2}\mathcal{A}^\mu) - (m + g_\sigma\sigma)]\psi \\ & + \frac{1}{2}\partial_\mu\sigma\partial^\mu\sigma - U(\sigma) - \frac{1}{4}\Omega_{\mu\nu}\Omega^{\mu\nu} + \frac{1}{2}m_\omega^2\omega^2 \\ & - \frac{1}{4}\vec{R}_{\mu\nu}\vec{R}^{\mu\nu} + \frac{1}{2}m_\rho^2\vec{\rho}^2 - \frac{1}{4}F_{\mu\nu}F^{\mu\nu} , \end{aligned} \quad (1)$$

where $\Omega_{\mu\nu} = \partial_\mu\omega_\nu - \partial_\nu\omega_\mu$, $\vec{R}_{\mu\nu} = \partial_\mu\vec{\rho}_\nu - \partial_\nu\vec{\rho}_\mu$ and $F_{\mu\nu} = \partial_\mu\mathcal{A}_\nu - \partial_\nu\mathcal{A}_\mu$ are the field tensors. In Eq. (1), the arrow above a symbol indicates the isovector character of the corresponding field. The term $U(\sigma) = \frac{1}{2}m_\sigma^2\sigma^2 + \frac{1}{3}g_2\sigma^3 + \frac{1}{4}g_3\sigma^4$ contains the selfinteractions of the σ field, added according to [31]. The bare hadron masses m , m_σ , m_ω and m_ρ , coupling constants g_σ , g_ω , g_ρ and the non-linear parameters g_2 and g_3 have been adopted from the $NL3^*$ parametrization of the non-linear Walecka model, which gives reasonable values for the incompressibility modulus, $K_\infty = 258$ MeV, and the nucleon Dirac effective mass $m^* = 0.594m$ at the saturation density $\rho_0 = 0.150$ fm $^{-3}$ of nuclear matter [32]. The $NL3^*$ parametrization is the modification of the well known $NL3$ set of parameters [33]

adjusted to describe the ground state properties of both spherical and deformed nuclei as well as the GMR energies of heavy nuclei. The momentum dependence of the proton-nucleus optical potential, studied recently in Ref. [34], is of minor importance here.

The theoretical description of heavy-ion collisions is realized within the GiBUU transport approach [29], which is based on a relativistic kinetic equation. Thorough derivations of the transport equation from an effective hadron-meson field theory [30], can be found elsewhere [35]. The relativistic kinetic equation reads

$$(p^{*0})^{-1} \left[p^{*\mu} \partial_\mu^x + \left(p_\mu^* F_i^{k\mu} + m^* \partial_x^k m^* \right) \partial_k^{p^*} \right] f_i(x, \mathbf{p}^*) = \sum_{j=n,p} I_{ij} \quad (2)$$

with $\mu = 0, 1, 2, 3$ and $k = 1, 2, 3$. The l.h.s. of Eq. (2) describes the classical Vlasov propagation of a one-body phase space distribution function $f_i(x, \mathbf{p}^*)$ for protons and neutrons ($i = p, n$) in the mean meson fields. This is expressed in terms of a kinetic four-momentum $p^* = p_i - V_i$, where p_i is the canonical four-momentum, of the field tensor $F_i^{\mu\nu} = \partial^\mu V_i^\nu - \partial^\nu V_i^\mu$, and of the Dirac effective mass $m^* = m + S$. Here V_i^μ and S are the vector¹ and scalar field, respectively.

$$V_i^\mu = g_\omega \omega^\mu + g_\rho \tau_i^3 \rho^{3\mu} + \frac{e}{2} (1 + \tau_i^3) \mathcal{A}^\mu, \quad (3)$$

$$S = g_\sigma \sigma, \quad (4)$$

where $\tau_i^3 = +(-)1$ for $i = p(n)$.

The particles are assumed to be on the Dirac effective mass shell, i.e.

$$p^{*0} = \sqrt{m^{*2} + \mathbf{p}^{*2}}. \quad (5)$$

In fact, the GiBUU model propagates not only nucleons, but also all resonances up to the mass of 2 GeV, as well as mesons, e.g., pions, kaons. However, in the present study we will concentrate only on the nucleonic degrees of freedom. In this case, the collision terms in the r.h.s. of Eq. (2) are the Uehling-Uhlenbeck collision integrals describing elastic nucleon-nucleon scattering:

$$I_{ij} = \int \frac{2d^3p_2^*}{(2\pi)^3} \int d\sigma_{ij}(\mathbf{p}_1^*, \mathbf{p}_2^*; \mathbf{p}_{1'}^*, \mathbf{p}_{2'}^*) v_{12} \\ \times [f_i(\mathbf{p}_{1'}^*) f_j(\mathbf{p}_{2'}^*) \bar{f}_i(\mathbf{p}_1^*) \bar{f}_j(\mathbf{p}_2^*) - f_i(\mathbf{p}_1^*) f_j(\mathbf{p}_2^*) \bar{f}_i(\mathbf{p}_{1'}^*) \bar{f}_j(\mathbf{p}_{2'}^*)], \quad (6)$$

¹ Assuming that there is no mixing between proton and neutron states, the 1-st and 2-nd isospin components of the ρ -meson fields vanish.

where the time-space argument x of the distribution functions is dropped for brevity and $\mathbf{p}_1^* \equiv \mathbf{p}^*$. The hole distribution functions are denoted as $\bar{f}_i(\mathbf{p}^*) \equiv (1 - f_i(\mathbf{p}^*))$. Thus the final state Pauli blocking is explicitly included in (6). The collision integral (6) depends on the differential elastic scattering cross section $d\sigma_{ij}(\mathbf{p}_1^*, \mathbf{p}_2^*; \mathbf{p}_{1'}^*, \mathbf{p}_{2'}^*)$ with initial momenta $\mathbf{p}_1^*, \mathbf{p}_2^*$ and final momenta $\mathbf{p}_{1'}^*, \mathbf{p}_{2'}^*$, and on the relative velocity v_{12} of colliding nucleons. We use in this work the energy- and angular-dependent vacuum nucleon-nucleon cross sections (see [26] for details).

An exact solution of the set of the coupled transport equations for the different hadrons is not possible. Therefore, the commonly used test-particle method for the Vlasov part is applied, whereas the collision integral is modeled in a parallel-ensemble Monte-Carlo algorithm. The GiBUU transport model has not been applied to low energy reactions so far. An important requirement here is a very good description of the ground state of a nucleus in test particle method, which is the topic of the next chapter.

III. IMPROVED METHOD FOR NUCLEAR GROUND STATES IN GIBUU

Practically all existing nuclear kinetic transport models based on the test particle technique (c.f. [20, 21, 23, 29] and refs. therein), including GiBUU, use the same method of the nuclear ground state preparation. Typically, the coordinates of test particles are sampled according to empirical Woods-Saxon or even uniform density profiles, while the test particle momenta are distributed with the help of a local density approximation. The standard numerical treatment of the transport equation works well for high energy reactions, in which several collective flow observables are described quantitatively well [36]. However, in low energy reactions the memory of the exit channel to the initial configuration is important. A disadvantage of standard numerical treatments is that the initial distribution functions of protons and neutrons deviate from the corresponding static solutions of the Vlasov equation. Therefore, nuclei are not initialized in their proper ground states. This makes their dynamical propagation unstable. Another source of spurious instability is the numerical treatment of the Pauli blocking, which mainly influences the momentum space of the test particles in full BUU simulations.

A. Phase space initialization

We improve the phase space initialization of ground state nuclei in the transport model in the following way: the nuclear ground state is described in a semi-classical treatment, in which the density distribution of a spherical ground state nuclei is obtained by minimizing the energy functional. In RMF, the energy functional corresponds to the relativistic Hamiltonian density, which is obtained from the T^{00} -component of the energy-momentum tensor. The same functional is then used for the propagation of the system. In calculations of the time evolution, we neglect the time derivatives of the mean mesonic fields and of the electromagnetic field in the Lagrangian (1). For the mean mesonic fields, this should be a reasonable approximation, since the time scale of the GMR motion $\sim 40 - 80$ fm/c (c.f. Fig. 7 below) is much larger than the time scale of the free field oscillations $\sim 1/m_{\text{mes}} = 0.2 - 0.4$ fm/c, where $m_{\text{mes}} \sim 0.5 - 0.8$ GeV is a meson mass. For the electromagnetic field, neglecting time derivatives corresponds to disregarding a radiation. The last could be, in-principle, treated in terms of a quantum transition probability. However, in the specific case of 0^+ transitions, the electromagnetic radiation is suppressed [37]. The space components of electromagnetic field are also neglected, i.e. $\mathcal{A} \equiv (\mathcal{A}^0, 0, 0, 0)$. In the most calculations, in order to save CPU time, we also drop the space components of the vector meson fields. However, for completeness, the formalism below takes into account these components.

The RMF Hamiltonian density of the non-linear Walecka model reads:

$$\begin{aligned} \epsilon \equiv T^{00} = & \frac{2}{(2\pi)^3} \sum_{i=p,n} \int d^3p^* p_i^0(x, \mathbf{p}^*) f_i(x, \mathbf{p}^*) + \frac{1}{2}(\nabla\sigma)^2 + U(\sigma) \\ & - \frac{1}{2}[\nabla\omega^\mu\nabla\omega_\mu + m_\omega^2\omega^2 + \nabla\rho^{3\mu}\nabla\rho^3_\mu + m_\rho^2(\rho^3)^2 + (\nabla\mathcal{A}^0)^2] . \end{aligned} \quad (7)$$

The Hamiltonian density (7) takes into account the gradients of the meson fields in coordinate space according to [27]. This is important for description of surface effects, which is impossible in the usual local density approximation neglecting the gradient terms (c.f. [21, 26]). In distinction to the previous GiBUU calculations in the RMF mode, the isovector ρ -meson field and the Coulomb field \mathcal{A}_0 are explicitly included now.

The meson and electromagnetic field equations have the following form

$$\left(-\Delta + \frac{\partial U(\sigma)}{\partial \sigma}\right) \sigma = -g_\sigma \rho_S , \quad (8)$$

$$(-\Delta + m_\omega^2) \omega^\mu = g_\omega j_B^\mu , \quad (9)$$

$$(-\Delta + m_\rho^2) \rho^{3\mu} = g_\rho j_I^\mu , \quad (10)$$

$$-\Delta \mathcal{A}^\mu = e j_p^\mu . \quad (11)$$

The source densities and currents in the r.h.s. of Eqs. (8)-(11) are expressed in terms of the distribution functions as follows

$$\rho_S(x) = \frac{2}{(2\pi)^3} \sum_{i=p,n} \int d^3 p^* \frac{m^*}{p^{*0}} f_i(x, \mathbf{p}^*) , \quad (12)$$

$$j_i^\mu(x) = \frac{2}{(2\pi)^3} \int d^3 p^* \frac{p^{*\mu}}{p^{*0}} f_i(x, \mathbf{p}^*) , \quad (i = p, n) \quad (13)$$

$$j_B^\mu(x) = j_p^\mu(x) + j_n^\mu(x) , \quad (14)$$

$$j_I^\mu(x) = j_p^\mu(x) - j_n^\mu(x) . \quad (15)$$

In the static case, the distribution functions are Fermi distributions:

$$f_i^{\text{static}}(\mathbf{r}, \mathbf{p}^*) = \Theta(p_{F_i}(\mathbf{r}) - |\mathbf{p}^*|) . \quad (16)$$

The space components of the source currents (13)-(15) as well as those of the mesonic and electromagnetic fields disappear in a static system. Therefore, the Hamiltonian density (7) becomes a functional of proton and neutron densities $\rho_{p,n} = j_{p,n}^0$ only.

The RTF equations for a static nucleus with Z protons, N neutrons and $A = N + Z$ nucleons are obtained by applying a variational principle to the total energy $E = \int \epsilon[\rho_p, \rho_n] d^3 r$ under the constraint of particle number conservation:

$$\delta \int (\epsilon[\rho_p, \rho_n] - \mu_p \rho_p(\mathbf{r}) - \mu_n \rho_n(\mathbf{r})) d^3 r = 0 . \quad (17)$$

The chemical potentials for protons and neutrons, $\mu_{p,n}$, are fixed by the conditions

$$Z = \int \rho_p(\mathbf{r}) d^3 r , \quad N = \int \rho_n(\mathbf{r}) d^3 r . \quad (18)$$

Substituting the Hamiltonian density functional (7) in Eq. (17) leads to the RTF-equations for protons and neutrons:

$$g_\omega \omega^0 + g_\rho \rho^{30} + e \mathcal{A}^0 + E_{F_p}^* = \mu_p , \quad (19)$$

$$g_\omega \omega^0 - g_\rho \rho^{30} + E_{F_n}^* = \mu_n , \quad (20)$$

where $E_{F_{p,n}}^* = \sqrt{p_{F_{p,n}}^2 + m^{*2}}$. For a spherical nucleus, the RTF equations (19,20) together with the field equations (8)-(11) completely determine the radial dependence of the proton and neutron densities and fields, i.e. $\rho_{p,n}(r)$, $\sigma(r)$, $\omega^0(r)$, $\rho^{30}(r)$ and $\mathcal{A}^0(r)$. The densities are obtained as the selfconsistent solution of Eqs. (8-11,18-20), with $p_{F_i} = (3\pi^2\rho_i)^{1/3}$ ($i = p, n$) according to the local density approximation. This method then yields a consistent description of the groundstate. The densities are realistic but somewhat too steep in the surface region.

The solution of the RTF equations gives the nuclear density $\rho_i(r)$ and the local Fermi-momentum $p_{F_i}(r)$ ($i = p, n$). The test particles for the numerical solution of the transport equation are distributed according to these functions. The propagation of the system is described by the test particle equations of motion, which directly follow from the transport equation (2) by putting its r.h.s. equal to zero and read ($j = 1, \dots, A \cdot \mathcal{N}$ with \mathcal{N} being the number of test particles per nucleon):

$$\dot{\mathbf{r}}_j = \frac{\mathbf{P}_j^*}{p_j^{*0}} \quad (21)$$

$$\dot{p}_j^{*k} = \frac{p_{j\mu}^*}{p_j^{*0}} F_j^{k\mu} + \frac{m_j^*}{p_j^{*0}} \partial^k m_j^* . \quad (22)$$

At each time step of the simulation, the scalar density (12) and currents (13)-(15) are calculated on a grid in coordinate space. Using these quantities, the equations of motion for the meson and Coulomb fields (8)-(11) are solved numerically. Note, that the solution of Eq. (8) requires some more iterations, since the scalar density ρ_S in its r.h.s depends itself on the σ meson field via the effective mass m^* .

The collision term in the r.h.s. of Eq.(2) is simulated by explicit two-body collisions between test particles using the geometrical collision criterium (c.f. [26] for details). An important feature here is the numerical treatment of the Pauli blocking, which is discussed in detail below.

B. Pauli blocking

The frequency of two-body collisions in a Fermi gas depends on the occupancies of the scattering final states via the hole distribution functions \bar{f}_i (see Eq.(6)). By the energy and momentum conservation, no collisions take place at zero temperature, when $f_i(\mathbf{r}, \mathbf{p}^*) =$

$\theta(p_{F_i}(\mathbf{r}) - |\mathbf{p}^*|)$. In test-particle simulations, however, it is impossible to model the exact $T = 0$ Fermi distribution. This causes some spurious two-body collisions even in the ground state nucleus. The magnitude of this spurious effect crucially depends on a numerical technique of the Pauli blocking calculation. In the standard GiBUU [29, 38], the occupation number $f_i(\mathbf{r}, \mathbf{p}^*)$ is calculated by counting the number of test particles in the phase space volume element composed of small spherical volumes ΔV_r with radius r_r centered at \mathbf{r} in coordinate space and ΔV_p with radius r_p centered at \mathbf{p}^* in momentum space:

$$f_i(\mathbf{r}, \mathbf{p}^*) = \sum_{j: \mathbf{p}_j^* \in \Delta V_p} \frac{1}{\kappa (2\pi\sigma^2)^{3/2}} \int_{\Delta V_r, |\mathbf{r} - \mathbf{r}_j| < r_c} d^3r \exp\left\{-\frac{(\mathbf{r} - \mathbf{r}_j)^2}{2\sigma^2}\right\}, \quad (23)$$

where

$$\kappa = \frac{2 \Delta V_r \Delta V_p \mathcal{N}}{(2\pi)^3} \frac{4\pi}{(2\pi\sigma^2)^{3/2}} \int_0^{r_c} dr r^2 \exp\left\{-\frac{r^2}{2\sigma^2}\right\} \quad (24)$$

is a normalization factor. In Eq.(23), the sum is taken over all test particles j of the type $i = p, n$ whose momenta belong to the volume ΔV_p . In the coordinate space, the test particles are represented by Gaussians of the width σ cutted-off at the radial distance r_c . The default values of parameters are $r_p = 80$ MeV/c, $r_r = 1.86$ fm, $\sigma = 1$ fm, $r_c = 2.2$ fm. This set of parameters is a compromise between the quality of the Pauli blocking in the ground state and the smallness of statistical fluctuations in the case of simulations with $\mathcal{N} \sim 200$ test particles per nucleon. Typically, this is good enough for modeling the heavy-ion collisions at the beam energies above ~ 100 MeV/nucleon. In the case of a small-amplitude dynamics near nuclear ground state, the accuracy provided by Eqs.(23),(24) is not enough, when the default parameters are used. The main reason is the constant, i.e. momentum-independent radius r_p , which introduces a spurious temperature of the order of several MeV. To reduce this effect, we have introduced the coordinate- and momentum-dependent radius of the momentum space volume ΔV_p as $r_p(\mathbf{r}, |\mathbf{p}^*|) = \max(20 \text{ MeV}/c, p_{F_i}(\mathbf{r}) - |\mathbf{p}^*|)$, which provides a sharper momentum dependence near Fermi momentum. The calculations of the present work are performed with $\mathcal{N} = 1000 - 10000$. This allows us to use the reduced parameters also in the coordinate space: $r_r = 0.9 - 1.86$ fm, $\sigma = 0.5$ fm, $r_c = 1.1$ fm. The calculations with the default and modified set of parameters for the Pauli blocking are compared in the following Sect. IV.

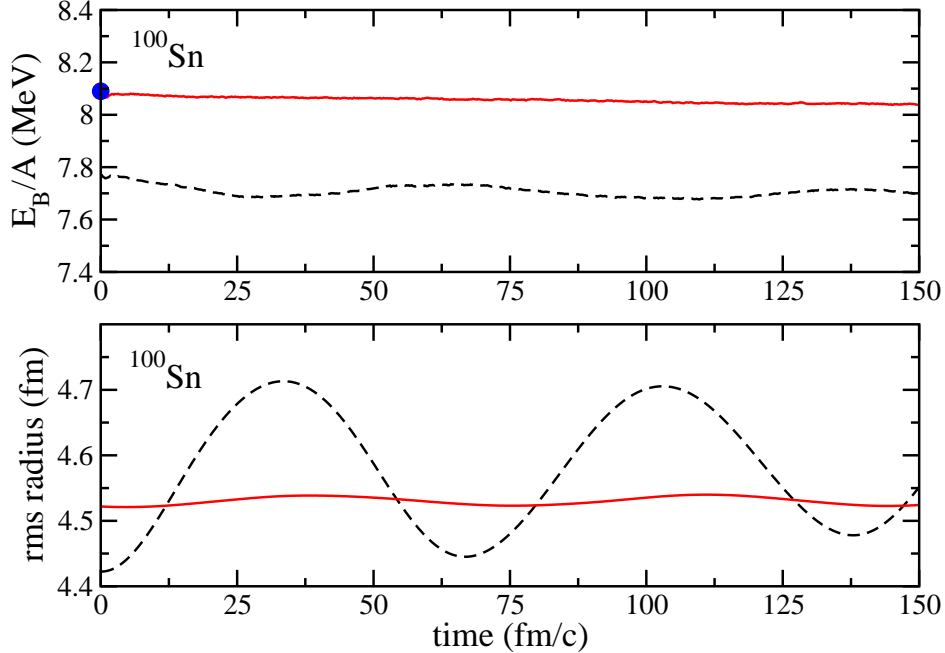


FIG. 1: (Color online) Time evolution of the binding energy per nucleon (panel on the top) and root mean square (rms) radius (panel on the bottom) for a ground state ^{100}Sn nucleus. Vlasov calculations using the (dashed) standard initialization and the (solid) improved initialization are shown. The filled circle in the top panel at $t = 0$ fm/c gives the RTF-value of the binding energy.

IV. RESULTS

We study first the influence of the initialization method on the temporal evolution of nuclei in their ground states. The improved transport model is applied then to the dynamics of low energy nuclear excitations, which are simulated by initializing slightly expanded nuclei. We present results from pure Vlasov and full BUU calculations for different nuclei. If not indicated elsewhere, for the Vlasov calculations 10000 test particles per nucleon were used. The full BUU calculations were performed with 1000 test particles due to time limitations.

A. Stability of the ground state

Fig. 1 shows the time evolution of the binding energy per nucleon and the root mean square (rms) radius of a ground state ^{100}Sn nucleus. The standard initialization method using the empirical Woods-Saxon density distribution produces the binding energy smaller by 0.3-

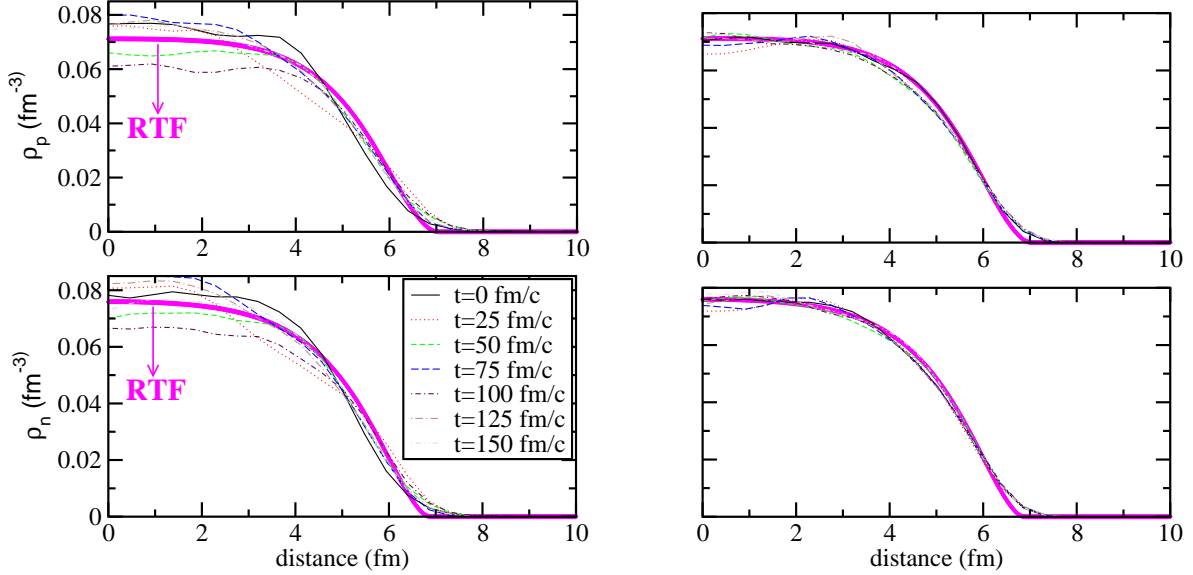


FIG. 2: (Color online) Density profiles of protons (panels on the top) and neutrons (panels on the bottom) for the same nucleus as in Fig. 1. The thick curves are RTF calculations. The other curves show density distributions from the Vlasov dynamics at different times (as indicated) using the standard initialization (panels on the left) and the improved one (panels on the right).

0.4 MeV/nucleon with respect to the RTF value of $E_B/A \simeq 8.1$ MeV. This is expected, since the minimum of the total energy is not reached by the standard initialization. The binding energy varies with time due to numerical errors in the solution of the time evolution equations (21),(22) and field equations (8)-(11). For the standard initialization, the rms radius reveals quite strong fluctuations, comparable in the amplitude with the true GMR vibrations (see Fig. 6). These artificial temporal oscillations lead also to a significant particle loss with increasing time, if collisions are included (see below). Applying the improved initialization, in which the same Hamiltonian density functional is used for both the initialization of the nucleus and its temporal propagation, the situation becomes considerably better. At $t = 0$ fm/c the value of the binding energy per nucleon agrees with the corresponding RTF value, and the rms radius stays almost constant in time.

A more detailed picture of the Vlasov calculations with the standard and the improved initialization method is shown in Fig. 2 in terms of the proton and neutron density distributions. Using the standard initialization (figures on the left panel) the initial ($t = 0$ fm/c) density profiles do not fit that one of RTF. This leads to significant density oscillations

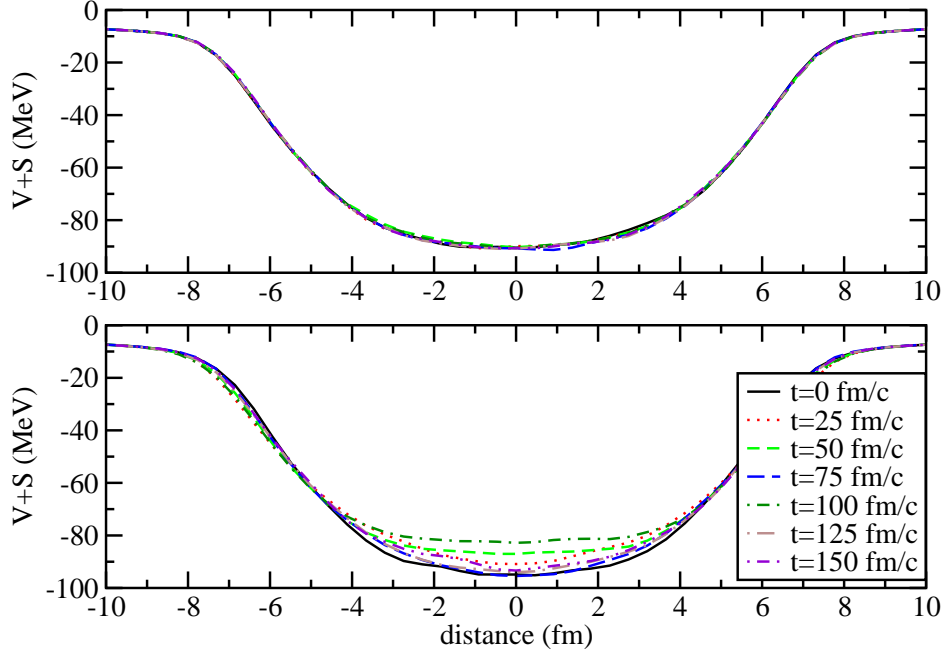


FIG. 3: (Color online) The proton mean field potential $V^0 + S$ (see Eqs. (3, 4)) along the z -axis passing through the center of the ^{100}Sn nucleus. The different curves show the Vlasov results at different times (as indicated) using the improved initialization (upper panel) and the standard one (lower panel).

around the true ground state density profiles (RTF) with the result of spurious oscillations in the rms-radius of the system (see again Fig. 1). A consistent treatment between the ground state nucleus and its propagation leads to very good stable configurations, see graphs on the right panel of Fig. 2.

We remind that in relativistic transport studies the central mean-field potential arises from the sum of the large negative Lorentz scalar and large positive Lorentz vector potentials. Thus, small spurious variations in density cause strong numerical fluctuations in the mean-field potential. This is demonstrated in Fig. 3, where the mean field potential is displayed as a function of the coordinate along the central z -axis. The Vlasov calculations with the standard initialization (panel on the bottom) show large fluctuations of the order of 10%, while these fluctuations almost vanish in the calculations using the improved initialization method.

Including two-body collisions requires a careful implementation of the Pauli blocking to prevent the ground state to be destroyed. To give an impression of how well it is working

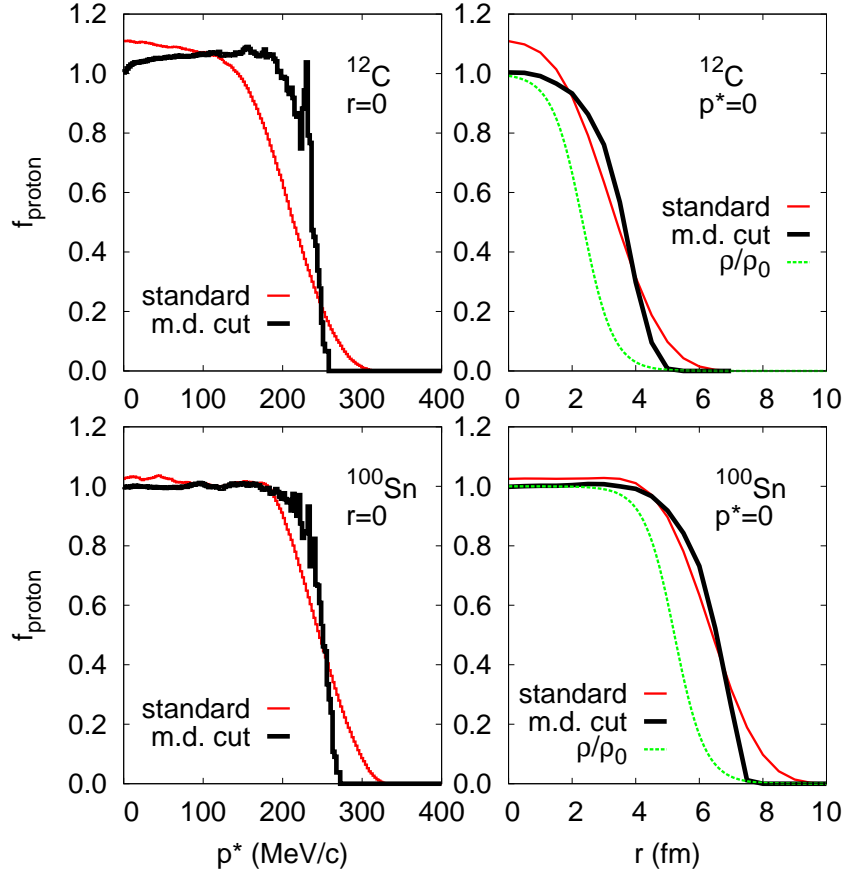


FIG. 4: (Color online) Momentum dependence of the proton occupation number f_{proton} in the center of ^{12}C and ^{100}Sn nuclei is shown in the upper and lower left panels, respectively. Radial dependence of f_{proton} at the zero momentum for ^{12}C and ^{100}Sn is depicted in the upper and lower right panels, respectively. The results are presented for the standard (thin solid lines) and momentum-dependent (thick solid lines) radius r_p . The fluctuations of f_{proton} near Fermi momentum $p_F \simeq 250$ MeV/c are due to finite number of test particles per nucleon which was set to 10000 in this calculation. The nucleon density in units of ρ_0 is shown additionally by dashed lines in the right panels. We see that at the half-central-density radius, the proton occupation number is only about 10% below unity.

in our test particle calculations, Fig. 4 shows the momentum (left) and radial (right) dependence of the proton occupation numbers, which are used in the evaluation of the Pauli blocking factors, for ^{12}C and ^{100}Sn nuclei. The calculation with the default parameters of a

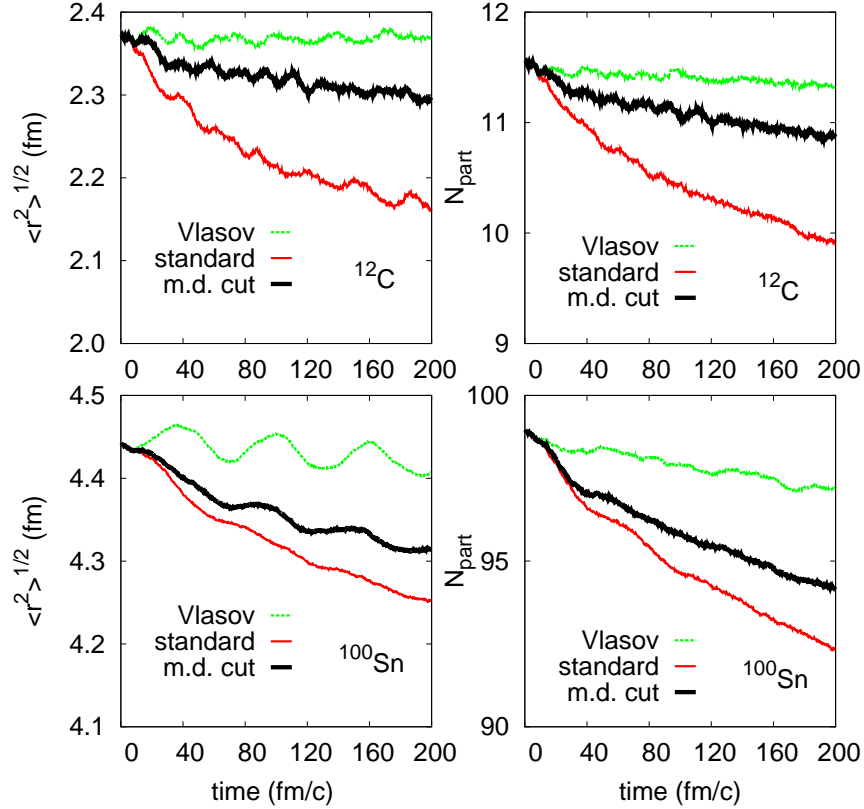


FIG. 5: (Color online) The nuclear rms-radius Eq.(26) (left panels) and the number of particles in the high-density region Eq.(25) (right panels) as a function of time for the ground state ^{12}C and ^{100}Sn nuclei. The Vlasov calculations are represented by dashed lines. The full BUU results with the standard and modified Pauli blocking parameters are shown by thin and thick solid lines, respectively.

Pauli blocking produces a rather diffuse momentum dependence, especially for the light ^{12}C nucleus. Using the momentum-dependent radius r_p and the reduced width of a Gaussian, as explained in subsect. III B, largely improves the momentum dependence of occupation numbers near Fermi momentum. The radial dependence of the occupation numbers also becomes closer to the step function, when the calculation is done with the modified Pauli blocking parameters.

To demonstrate the effect of Pauli blocking parameters on the ground state evolution, in Fig. 5, we present the time dependence of the rms-radius of a nucleus (left) and of the number of particles in the high-density, $\rho > \rho_{\text{min}}$, space region (right) for the carbon and tin

nuclei. Explicitly, these quantities have been calculated as

$$N_{\text{part}} = \int_{\rho > \rho_{\text{min}}} d^3r \rho(\mathbf{r}) \quad , \quad (25)$$

$$\langle r^2 \rangle = N_{\text{part}}^{-1} \int_{\rho > \rho_{\text{min}}} d^3r r^2 \rho(\mathbf{r}) \quad (26)$$

with $\rho_{\text{min}} = 0.1\rho_0$. Vlasov calculations practically conserve the number of particles in the high density region and produce almost constant in time rms-radii. The spurious effect of two-body collisions in the ground state nuclei leads to the particle emission to vacuum which amounts after 200 fm/c to about 10% of the total mass number in the case of standard Pauli blocking parameters and $\sim 5\%$ in the case of the modified parameters. Correspondingly, the rms-radius gets reduced. This spurious reduction has to be excluded in the calculation of the rms-radius in full BUU simulations, as discussed later on. Below, we will always apply the modified Pauli blocking parameters as explained in subsect. III B.

B. Giant Monopole Resonance: GiBUU calculations

The different methods of initialization of nuclear ground states influence the dynamical calculations of excited nuclei. We will model the low energy nuclear giant monopole collective excitations by initializing an expanded nucleus at $t = 0$ fm/c. This is realized by re-scaling the coordinates of the test particles such that the corresponding excitation energy is close to the experimental values. The relation between the scaling parameter and the excitation energy is obtained by expanding the energy per nucleon E/A around saturation density or the ground state radius R_0 :

$$E/A(R) \simeq E_0/A + \frac{1}{2}K_\infty \left(\frac{R - R_0}{R_0} \right)^2 \quad . \quad (27)$$

With $K_\infty = 258$ MeV and using the experimental values [2] for the excitation energy $\Delta E = E - E_0$ one obtains scaling parameters $\Delta R/R = (R - R_0)/R_0$ in the range of $\approx 0.03 - 0.05$ for $A \in (56, 208)$. The system is then propagated either without (Vlasov mode) or with (BUU mode) collisions between the nucleons of the excited nucleus.

Fig. 6 shows the time evolution of a ^{100}Sn nucleus using the different prescriptions of initialization.

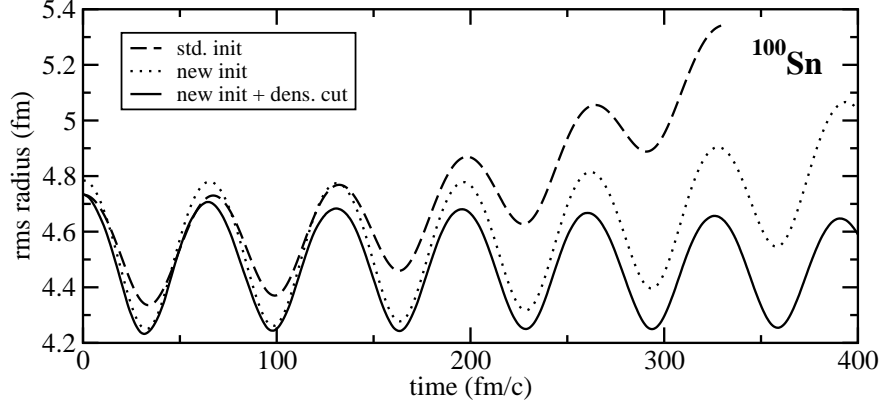


FIG. 6: (Color online) Time dependence of the rms-radius for the excited ^{100}Sn nucleus. The meaning of the different curves is explained in the text. The calculations are done in the Vlasov mode.

The standard method does not provide stable solutions and the rms-radius of the ^{100}Sn -nucleus explodes for $t > 200 \text{ fm}/c$ due to strong particle loss. The situation is considerably improved in the new initialization. A clear oscillation signal can be seen with a particle emission for very late times ($t > 275 \text{ fm}/c$) which is, however, only moderate. Emitted particles increase the rms-radius of the total nuclear system which hinders the true oscillation signal. They have to be excluded, therefore, in the calculation of the rms-radius of an oscillating nucleus when extracting the excitation energy and width of the GMR. We thus consider only particles at densities higher than $0.1\rho_0$ according to Eqs.(25),(26). After this correction we obtain a clear signal for the resonance. The period of the oscillation characterizes the frequency and thus the excitation energy of the resonance, and an exponential damping (see below) — its finite lifetime.

We have performed pure Vlasov mode calculations for different excited nuclei and analyzed the results in terms of the time dependence of the rms-radius, as seen in Fig. 7. With increasing mass number the frequency of the oscillation decreases and thus also the excitation energy. An exponential damping is visible, even without the inclusion of collisional effects. This effect has been interpreted as a wall friction [39, 40], and it will be discussed later. An important feature in the study of nuclear collective excitations is the calculation of the lifetime or the width of the different multipole modes of the nuclear excitation. TDHF theory and Vlasov dynamics does not include any collisional broadening effects.

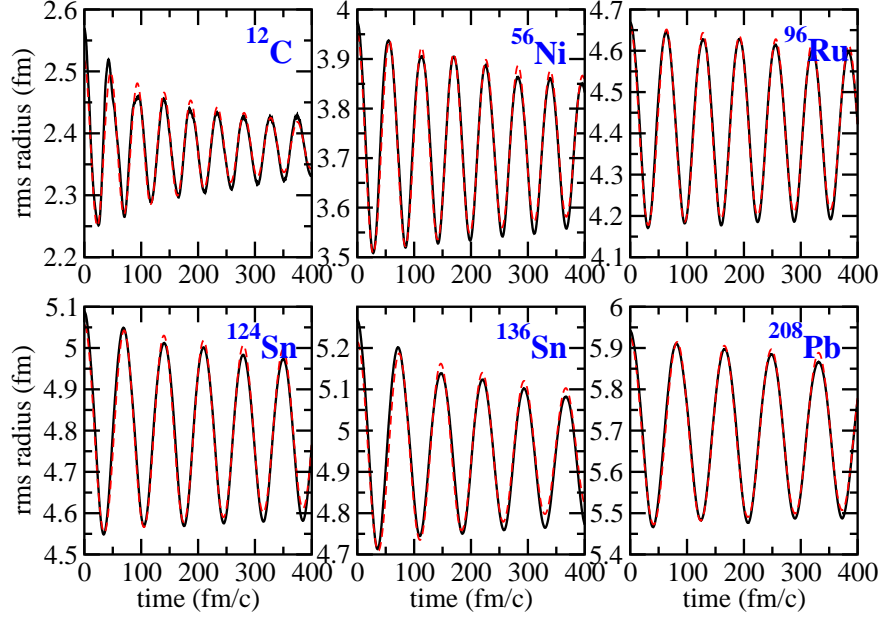


FIG. 7: (Color online) Time dependence of the rms-radius for different nuclei, as indicated. (Solid) Vlasov calculations, (dashed) fit according to Eq. (29).

The nuclear collective dynamics of giant multipole vibrations in the ground state nuclei has not been so far investigated within the full BUU equation, mainly due to the reasons of a ground state instability. With the improved initialization method the Vlasov propagation of a ground state is almost perfect. The numerical procedure of the Pauli blocking in a full BUU ground state simulation is improved by applying the modifying method, but is still far from being exact. This situation leads to a spurious particle emission in ground state BUU calculations and thus to a spurious escape width Γ_{es} , which impedes the determination of the total width.

The spurious contribution to the total width has therefore to be excluded, as explained in Fig. 8, where the time evolution of bound particles for a nucleus in its ground state (dashed curve) and in the GMR mode (solid curve) is shown. Already in the ground state, particles leave the nucleus due to spurious two-body collisions resulting in a spurious escape width Γ_{es} . On the other hand, the BUU simulation for the excited nucleus contains also an escape width which is very similar to that of the ground state. Assuming Γ_{es} to be the same for

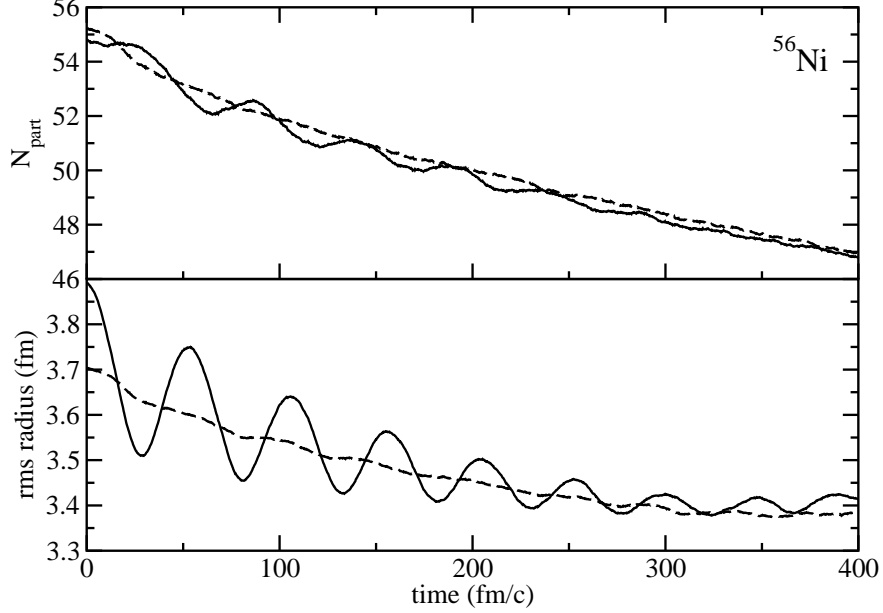


FIG. 8: (Color online) Time dependence of the number of particles in high-density region (top panel) and the r.m.s. radius (bottom panel) defined according to Eqs. (25),(26) for a ^{56}Ni nucleus. Dashed lines: ground state BUU calculation, solid lines: BUU calculation for an excited ^{56}Ni nucleus in the GMR mode.

both ground state and excited state we can make the following Ansatz:

$$\begin{aligned}
 N_{gs}(t) &= N_0 \exp(-\Gamma_{es}t) \quad \text{for the ground state} \\
 N_{exc}(t) &= N_0 \exp(-\Gamma_{es}t)F(t) \quad \text{for the excited GMR state} \quad , \quad (28)
 \end{aligned}$$

where N_0 is the number of particles at $t = 0$ fm/c and $F(t)$ is a fit function for the oscillation signal, which contains the stochastic collisional width:

$$F(t) = \alpha + \beta \cos(\omega t + \delta) \exp(-\gamma t) \quad . \quad (29)$$

The spurious width can be excluded by taking the ratio of N_{gs} and N_{exc} , or their difference in the case of very small value of Γ_{es} . The latter method is applied here in extracting the GMR width, since $\Gamma_{es} \sim 0.044, 0.045$ MeV for a ground state and an excited nucleus, respectively. Thus, the physical escape width (relative to that in the ground state) is almost negligible, and we obtain the total width in full BUU calculations by a fit according Eq. (29) to the so-called corrected r.m.s. radius defined as

$$\langle r_{corr}^2 \rangle^{1/2}(t) = \langle r_{exc}^2 \rangle^{1/2}(t) - \langle r_{gs}^2 \rangle^{1/2}(t) + \langle r_{gs}^2 \rangle^{1/2}(0) \quad , \quad (30)$$

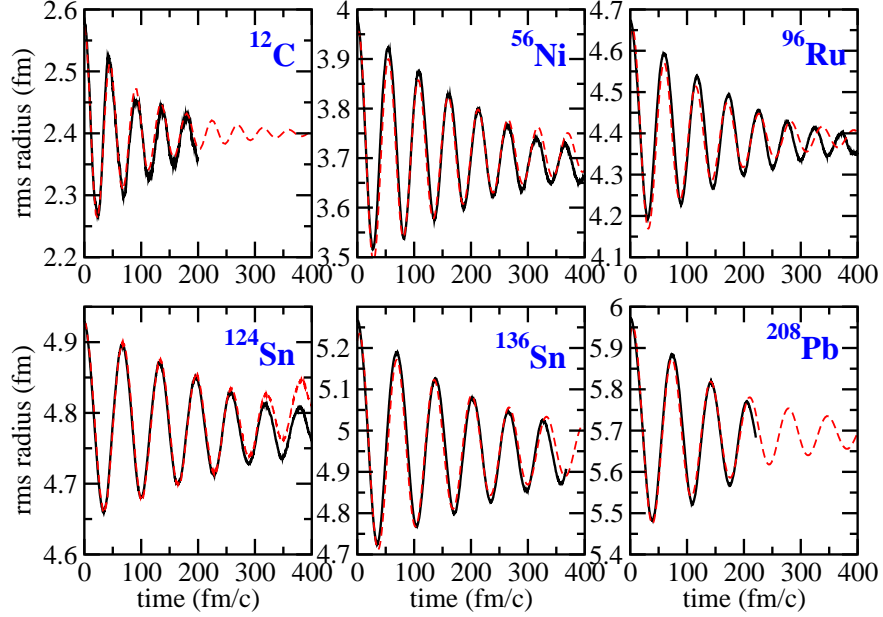


FIG. 9: (Color online) The corrected r.m.s. radius of Eq. (30) plotted as a function of time for different nuclei — solid lines. Calculations are done in the full BUU mode. The fit according to Eq. (29) is shown by the dashed lines.

where the depletion due to spurious particle loss is subtracted. However, the damping rate γ of the corrected r.m.s. radius oscillations is still somewhat influenced by an imperfect Pauli blocking procedure, which makes some uncertainty in our calculations of the GMR width. We also have checked the consistency of the extracted results on E^* and Γ obtained with the subtraction method by performing additional Fourier analyses of $\langle r^2 \rangle^{1/2}(t)$ before and after the correction. Lorentzian fits to the Fourier spectra lead to values for the width, which are the same with those extracted with the subtraction method. Also the excitation energy is not essentially affected. However, the excitation energy in full BUU calculations is slightly above the corresponding values in Vlasov mode. This effect is due to the spurious particle emission in full BUU calculations, which is furthermore related to the collective response of a smaller system.

The results for the corrected r.m.s. radius produced by full BUU calculations for different nuclei are shown in Fig. 9. Again, a clear oscillation signal is visible, however, due to the inclusion of collisions, a significant damping of the oscillations of the rms-radii appears, as compared to the pure Vlasov calculations of Fig. 7. We note, that in the case of a pure

Vlasov mode calculation, the difference between corrected and not corrected r.m.s. radii is negligibly small.

We have performed a fit to the results displayed in Figs. 7 and 9 according to Eq. (29) to obtain the centroid energies and the total width of the breathing mode. The results are summarized in Fig. 10 in terms of the excitation energy $E^* = \omega$ and the damping width $\Gamma = 2\gamma$ of the GMR, as a function of the mass number. The factor of two in the last formula is motivated by our intention to report the Full Width at Half Maximum (FWHM) of the GMR strength [17]. The gray band in the transport calculations for the width is an estimation related to the numerical uncertainty of the Pauli blocking factors. We first discuss the results obtained for E^* and then those for the width.

C. Giant Monopole Resonance: discussion

The theoretical Vlasov-calculations for the excitation energy scale with $A^{-1/3}$ and overestimate moderately the experimental data. The mass dependence is also consistent with TDHF calculations and with microscopic RPA studies [2]. Similar results for the excitation energy are obtained using full BUU calculations. It is a well known question, why relativistic structure calculations can explain the excitation energies of GMR with a higher value of the incompressibility modulus $K_\infty = 250 - 270$ MeV (c.f. refs. [10, 32, 41, 42]) than $K_\infty \simeq 220$ MeV deduced from nonrelativistic approaches [2] It has been shown in Ref. [41], that this is at least partly related to a stiffer density behaviour of the symmetry energy in RMF models with respect to the Skyrme-type effective interactions. On the other hand, the calculations of Ref. [10] have revealed the influence of differences in the surface compressibility in different RMF models on the GMR frequency. There is also another possible reason for differences between RMF and nonrelativistic approaches, which we address below.

Our calculations have been performed without nuclear Lorentz force, i.e., without taking into account the space-like components of the vector field.

We expect that a nonrelativistic Vlasov calculation, employing the same energy-density functional suitably parameterized, e.g. in a Skyrme form, will produce very similar results. To study the influence of the nuclear Lorentz force on the excitation energy (and the width) of the GMR, a Vlasov calculation explicitly taking into account the space-like components of the vector field has been performed for the lead-208 nucleus. The results are shown

TABLE I: Excitation energy E^* for a ^{208}Pb nucleus in different models: (Vlasov wLF) Vlasov calculation including the Lorentz force, (Vlasov) Vlasov calculation without the Lorentz force, (RPA) RPA calculations by Lalazissis et al. [32]. All the results are given in the case of NL3* model ($K_\infty = 258$ MeV).

| model | Vlasov | Vlasov wLF | RPA | exp. |
|-------------|--------|------------|------|----------------|
| E^* (MeV) | 15.2 | 14.2 | 13.9 | 13.7 ± 0.5 |

in table I and compared with other theoretical models of nuclear structure. First of all, the effect of the Lorentz force is negligible for the GMR width (not shown in the table). The excitation energy is moderately affected. In particular, a decrease of E^* by $\sim 6.5\%$ towards the experimental data and the relativistic structure calculations is observed, when the Lorentz force is included in the Vlasov calculation. We note that the same value for the compression modulus has been used in both Vlasov calculations. This result indicates the importance of the genuine relativistic effects when extracting the incompressibility modulus from GMR studies.

Another feature of interest in the transport results using both modes, full BUU and Vlasov, is the moderate decrease of the monopole frequencies with increasing neutron excess, as one can see in the results for E^* of Fig. 10 (upper panel) for the Sn-isotopes. Such a trend is also supported experimentally [43]. It is well known that the monopole frequencies are affected by the slope of the symmetry energy around saturation, as in detailed discussed in Ref. [44]. It would be a challenge to extend this transport study to particularly isospin asymmetric systems, such as the Sn-isotopes, where systematic experimental studies exist [43], and to investigate more exotic collective modes in neutron-rich systems.

To understand the GiBUU results on the mass dependence of the GMR centroid energy on a qualitative level, we have performed some simple estimations. As it is well known from empirical GMR systematics [1], the centroid energy of the GMR follows the $A^{-1/3}$ law:

$$E^* = \eta A^{-1/3} \quad . \quad (31)$$

This behaviour can be understood as a consequence of a sound-like excitation in a finite

system, i.e. $E^* = v_s k$, where v_s is a sound velocity and $k = \pi/R$ is the eigenvalue of the lowest compressional mode determined from the disappearance of the pressure at the free surface [45], $R = 1.2A^{1/3}$ is the nuclear radius. The hydrodynamical model [45] would give $v_s = (K_\infty/9m)^{1/2} \simeq 0.17$, which is the first sound velocity. Here, we have used the value of the incompressibility modulus $K_\infty = 258$ MeV provided by the NL3* model. The dependence $\eta \propto K_A^{1/2}$, where K_A is, however, the incompressibility modulus of the *finite nucleus*, is also provided by the scaling model of the GMR [2]. This model is usually applied in extraction of K_A from experimental data on GMR energy (c.f. [43]) by using the relation $E^* = \sqrt{K_A/m \langle r^2 \rangle}$, where $\langle r^2 \rangle \simeq 3R^2/5$ is the r.m.s. radius of the nucleus.

On the other hand, according to the Fermi liquid theory [46] the low-temperature collective excitations in the infinite system are of the zero sound type. It is well known, that the propagating zero sound type solutions of the dispersion relation for collisionless Fermi liquid at zero temperature exist only for the repulsive particle-hole interactions (c.f. [2]), which is not the case for the NL3* interaction used in the present work (see below). Introduction of finite temperature, generally, restore the collectivity for attractive particle-hole interactions, although it was proved only for momentum-independent interactions [47]. It is quite difficult, therefore, to actually identify the GMR vibration as the zero sound mode. Assuming, nevertheless, the nuclear matter zero sound nature of the GMR vibration, we can estimate the sound velocity as $v_s \simeq v_F = p_F/m_L^* \simeq 0.42$, where $p_F = 257$ MeV/c is the Fermi momentum at the nuclear matter saturation density and $m_L^* = \sqrt{m^{*2} + p_F^2} = 0.65m$ is the Landau effective mass in the case of the NL3* model.

As a result, one gets the values 90, 111 and 223 for the coefficient η in Eq. (31) for the hydrodynamical, scaling and zero sound pictures of the GMR, respectively. In the case of the scaling model, we assumed that $K_A = K_\infty$, which is a quite rough assumption. Generally, one has $K_A < K_\infty$ mostly due to the surface contribution [10]. It turns out (see the upper panel of Fig. 10), that Eq. (31) with the ‘‘hydrodynamical’’ value of $\eta = 90$ well fits the Vlasov results for large masses numbers $A \geq 100$, although the reason for this is not fully clear for us.

For light nuclei, as one can see from Fig. 10, the transport calculations overestimate the experimental data on E^* . This is the region where the RTF method becomes unreliable because the surface properties are not well described. However, the experimental determination of the GMR parameters in light nuclei is rather uncertain due to strong fragmentation

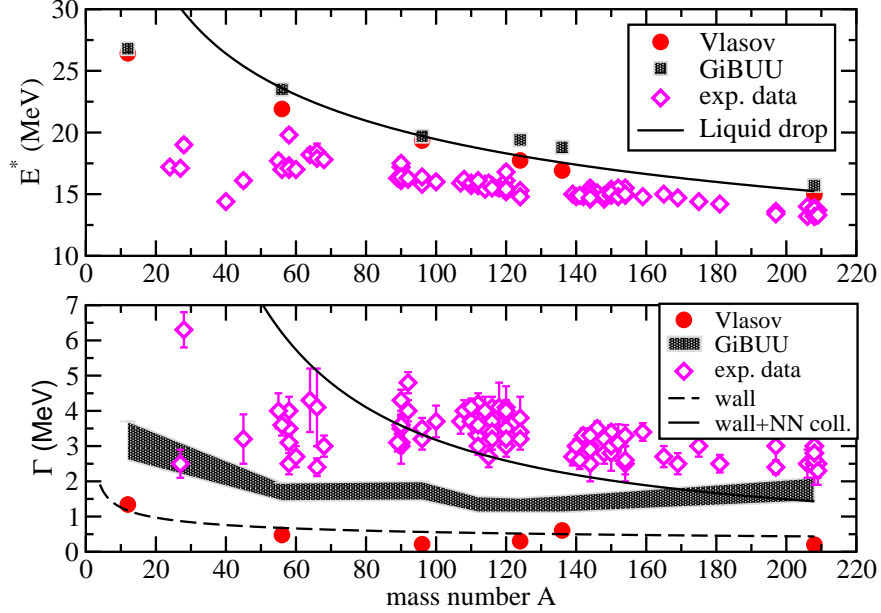


FIG. 10: (Color online) Excitation energy (upper panel) and width (lower panel) of the GMR as a function of the mass number. Vlasov and full GiBUU results (as indicated) are compared with experimental data (open diamonds). The solid line in the upper panel shows the fit by Eq.(31) with $\eta = 90$. In the lower panel, the dashed line depicts the fit of the Vlasov calculation using the wall formula (33) with $\xi = 20$, while the solid line shows the full width $\Gamma = -2\omega_I$ (see Eq.(35)) taking into account both the wall and collisional contributions. Experimental data are from Ref. [48].

of the 0^+ strength [1].

The situation for the width is more involved. Pure Vlasov calculations predict a very small value for the GMR width and do not fit the data, as expected. The inclusion of collisions in the full BUU calculations improves the comparison between theory and experiment considerably. The underprediction of the theoretical calculations to the data becomes smaller, but an exact agreement is not achieved. For a deeper interpretation of the GiBUU results on the mass dependence of the GMR width several additional analytical calculations were performed.

The width of a collective vibration is related to the dissipation processes. Within a pure mean field Vlasov calculation, the only damping mechanism is the one-body dissipation governed by a coupling of the single-particle and collective motions. Specifically for finite

systems, damping arises due to collisions of particles with a moving wall. This one-body dissipation leads to the following “wall” formula for the collective energy dissipation rate [39]

$$\dot{E} = m\rho\bar{v} \oint \dot{n}^2 d\sigma \quad , \quad (32)$$

where $\rho = \rho_p + \rho_n$ is the nucleon density, \dot{n} is the normal component of the wall velocity, and the integral is taken over the surface of a vessel. \bar{v} is the average speed of particles in the vessel. For cold nuclear matter one has $\bar{v} = \frac{3}{4}v_F$. The formula (32) is derived under strong simplifying assumptions of the gas at rest inside the vessel and of a sharp potential wall driven through the vessel. These conditions are usually assumed to be valid for small surface vibrations of the incompressible nuclear droplet [39], possibly with some modifications [40] (see also [17] and refs. therein). Application of the wall formula to the compressional modes is more questionable. Nevertheless by performing a rather simple calculation for the GMR mode within the liquid-drop model with a free surface we arrived to the usual formula for the one-body relaxation time (c.f. [17, 39])

$$\tau_{\text{wall}} = \frac{2R}{\bar{v}}\xi \quad , \quad (33)$$

with $\xi = 0.5$ which means an extremely strong dissipation. E.g., for ^{208}Pb we obtain the wall dissipation contribution to the GMR width $\Gamma_{\text{wall}} = 2/\tau_{\text{wall}} \simeq 17$ MeV. This result has to be considered as an extremely rough approximation. The self-consistency corrections, i.e. the collective motion of nucleons near the surface region [40] will modify Eq. (32) and τ_{wall} . Other effects like the surface diffuseness and curvature are not taken into account by the wall formula at all. Having these reservations in mind we will treat ξ in Eq. (33) as a free parameter and determine it from comparison with the results of calculations in a Vlasov mode. This produces the value $\xi \simeq 20$ as demonstrated in the lower panel of Fig. 10.

We will now discuss the two-body dissipation. It follows from the Uehling-Uhlenbeck collision integral that the two-body collisions take place only in the case of local deviations of the Fermi surface from a spherical shape or/and in the case of a finite temperature. Moreover, the relaxation rate of a nonequilibrated Fermi gas toward thermal equilibrium depends mainly on the total excitation energy and not on the concrete shape of a Fermi surface deformation [49]. In particular, in the linear approximation with respect to the deviation of a distribution function from the local equilibrium the relaxation rate is proportional to T^2 [46, 50]. This means, that collisional damping of a small Fermi surface distortions practically

vanishes at $T = 0$.

Thus collisional damping of a vibrational motion excited in the ground state nuclear system is practically absent at the beginning of time evolution and gradually switches on as some part of the collective vibrational energy is transferred to the heat. In Refs. [13, 14], an “apparent temperature” has been introduced in the calculation of the collisional widths of the giant quadrupole and giant dipole vibrations built on the ground state nuclei. The “apparent temperature” has been extracted in [13, 14] by subtracting the collective energy E_{coll} of a vibrational mode from the total excitation energy E^* : $T = \sqrt{(E^* - E_{\text{coll}})/a}$, where a is a level density parameter. This “temperature” has the real physical meaning only when the system reached a complete thermal equilibrium. Since the Pauli blocking factors in the Uehling-Uhlenbeck collision integral depend crucially on a temperature, calculations taking into account the time-dependent “apparent temperature” strongly increase the spreading width of a collective mode [13, 14] to a good agreement with experiment. In our estimates of the two-body dissipation we will use the upper limit for the “temperature” by putting $E_{\text{coll}} = 0$. For the level density parameter we will use the Fermi gas expression $a = \pi^2 A/4E_F$.

The GMR mode can be considered as a sound-like excitation inducing the Fermi surface distortions of all multipolarities $l \geq 2$ [17]. At $T \ll E_F$ the relaxation time of a small amplitude Fermi surface distortion with multipolarity $l \geq 2$ is (c.f. [17, 46, 50]) $\tau_l = \kappa_l/T^2$ where κ_l depends on the NN cross sections. The parameters κ_l have been computed in [19, 51] both for isovector and isoscalar vibrations for various choices of the NN cross sections. In the case of realistic energy and angular dependent vacuum NN cross sections this resulted in the following values of the isoscalar parameters: $\kappa_l = 868, 881$ and $401 \text{ MeV}^2\text{fm}/c$ for $l = 2, 3$ and $+\infty$, respectively. The case $l = +\infty$ corresponds to the relaxation of a single particle-hole configuration. For simplicity, we will set the same collisional relaxation time τ_{coll} for all multipolarities $l \geq 2$: $\tau_{\text{coll}} = \kappa/T^2$, where $\kappa = 3/(\kappa_2^{-1} + \kappa_3^{-1} + \kappa_\infty^{-1}) = 628 \text{ MeV}^2\text{fm}/c$. In the limit of large relaxation times the interrelationship between various sources of dissipation can be ignored [17] and one can treat also the wall dissipation as an additional source in the collision term by defining the total relaxation time as

$$\tau^{-1} = \tau_{\text{coll}}^{-1} + \tau_{\text{wall}}^{-1} . \quad (34)$$

Here we neglected the particle emission from an excited nucleus.

Applying the formalism of the linearized Landau-Vlasov equation in the relaxation time

approximation [17, 25] leads to the following approximate expression for the imaginary part ω_I of the giant multipole resonance frequency $\omega = \omega_R + i\omega_I$:

$$\omega_I \simeq -q\omega_R \frac{\omega_R\tau}{1 + q(\omega_R\tau)^2} \quad , \quad (35)$$

where the factor q is related with the Landau parameter F_0 as $q = 2/5(1 + F_0)$. Eq. (35) is, in fact, a suitable interpolation between the two well known limits [46] of rare collisions $\omega_R\tau \gg 1$ (zero sound) with $\omega_I \simeq -1/\tau$ and of frequent collisions $\omega_R\tau \ll 1$ (first sound) with $\omega_I \simeq -q\omega_R^2\tau$.

The Landau parameter F_0 can be expressed via the nuclear matter incompressibility K_∞ and Fermi energy $E_F = p_F^2/2m_L^*$ as $K_\infty = 6E_F(1 + F_0)$. The Landau effective mass m_L^* is connected to the Landau parameter F_1 as $m_L^* = m(1 + \frac{1}{3}F_1)$. Using the NL3* parameter set of the RMF model we obtain $F_0 = -0.20$ and $F_1 = -1.04$.

We have applied Eq. (35) with $\omega_R = E^*$ to compute the GMR width $\Gamma = -2\omega_I$. The result is shown by the solid line in the lower panel of Fig. 10. We observe that Eq. (35) gives a reasonable estimate of the magnitude of the collisional broadening for heavy nuclei. However the GMR width computed by using Eq. (35) is too large for medium and light nuclei. This is expected, given the fact that we have used the upper limit of the ‘‘apparent temperature’’, which becomes unphysically high for small mass numbers.

We have to point out that the zero sound damping conditions are valid for medium-to-heavy mass region $A > 50$, where we have $\omega_R\tau > 6$. This creates a puzzle, since, as we have seen above, the nuclear matter zero sound model would strongly overestimate the experimental GMR centroid energies. The answer could be, that the finite size effects essentially modify the zero sound mode in a real nucleus.

The GMR damping mechanism has been a long-winded problem in quantal structure calculations in the spirit of the RPA [52] and GCM calculations [10]. It is not the scope of this work to list all the various structure calculations and discuss their details, however, they can serve for a qualitative comparison with our calculations. For more details we refer to review articles [53, 54]. Fig. 11 displays again the GMR width in the Vlasov approach and the full BUU transport model and shows a comparison with the two sets of calculations from [55].

The (Q)RPA calculations, except for the contribution from pairing effects in open-shell nuclei, can be considered as the quantum analogue of our semiclassical Vlasov-mode cal-

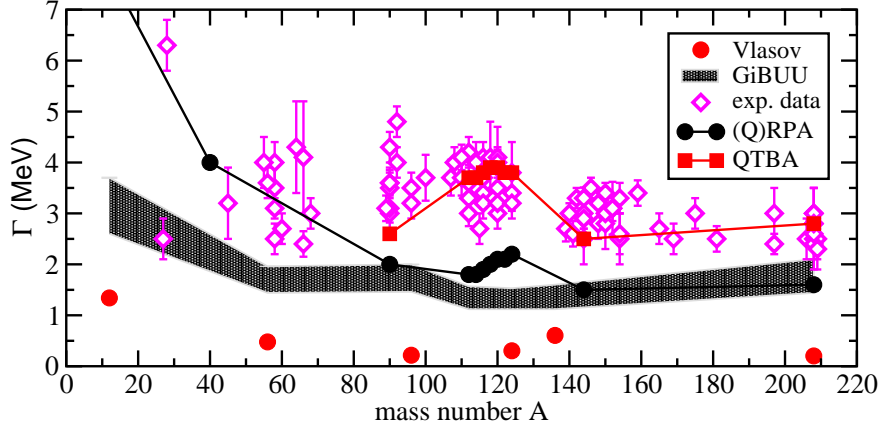


FIG. 11: (Color online) Width of the GMR as a function of the mass number. Vlasov and full GiBUU results (filled circles and gray band, respectively) are compared with experimental data (open diamonds) taken from [48]. The solid-circle and dashed-square curves shows the (Q)RPA and QTBA result, respectively, taken from Ref. [55].

culations. Collective response is a superposition of 1p-1h excitations in the both types of calculations. The difference between (Q)RPA and Vlasov results for the GMR width stems from missing the quantum fragmentation (Landau damping) width contribution in our calculations². Including a quasiparticle-phonon coupling in the quasiparticle time blocking approximation (QTBA) [55] can be regarded as a coupling to the 2p-2h configurations [56], which leads to the strong increase of the total GMR width. We observe a similar effect in our full BUU calculations, since nucleon-nucleon collisions in the Uehling-Uhlenbeck collision term also generate 2p-2h excited states. Moreover, the difference between QTBA and (Q)RPA results is quite close to the difference between full BUU and Vlasov results. This again indicates the importance of the correct description of the fragmentation width contribution.

In the spirit of refs. [15, 16], where the authors argue, that the Markovian approximation (i.e. a standard Uehling-Uhlenbeck collision term) is not able to produce any broadening of the giant multipole vibrations at zero temperature due to severe restrictions of the available phase space for two-body collisions, our result on the width enhancement by two-body

² In the analytical models based on BUU equation [17, 19] the quantum fragmentation width contribution has been included as an additional source term in kinetic equation. However, this is a pure phenomenological way to describe the damping width of giant multipole resonances in the ground state nuclei.

collisions looks quite surprising. In [16], the authors explain about 25-30% of the observed GMR width by taking into account the memory effects in collision term (non-Markovian approach). However, the analytical models [15–17, 19] are based on the linearized kinetic equation violating the energy conservation. In particular, the temperature increase due to the damping of collective motion is completely neglected in these approaches. We stress, that the solution of the full non-linear BUU equation in finite system leads to much stronger collisional broadening, than expected from the linearized models.

V. CONCLUSIONS AND OUTLOOK

The aim of the present work has been to study theoretically the excitation energy and the width of the giant monopole resonance in the framework of a semiclassical transport model. For this purpose, a description of nuclear ground states and their phase-space evolution within a unified semiclassical framework is indispensable. Nuclear ground states are described by the RTF method using a relativistic Hamiltonian density functional which, in particular, contains the space-derivatives of the mean meson fields. The proton and neutron densities from the RTF calculations serve to generate initial test particle configurations of different nuclei. The time evolution of the nuclear system is calculated by solving the kinetic equations which employ the mean-field potentials consistent with those used in RTF. The improved transport model gives a perfect stability of different ground state nuclei over long time scales in pure Vlasov dynamics.

The improved initialization method was found to be important to generate a clear signal of the breathing mode. Except for light nuclei, pure Vlasov calculations predict a mass dependence of the excitation energy which is consistent with available experimental data and with a simple liquid-drop model. The situation is, however, more complex concerning the lifetime of the breathing mode. Vlasov simulations strongly underpredict the experimental data on the GMR spreading width. The GMR width calculated by using the Vlasov equation behaves as $\propto A^{-1/3}$, which is consistent with the (modified) wall formula.

In order to better understand the GMR damping mechanism, the full transport calculations of the GMR mode have been performed for the first time. The inclusion of two-body collisions strongly enhances the total GMR width to a better agreement with experimental data. The strong damping of the GMR including the collision term can be understood in

terms of analytical models for one-body and two-body dissipation taking into account the temperature increase due to the dissipation of the GMR motion.

The Pauli blocking strongly influences the dynamics in full BUU calculations. Thus it has been treated as precise as possible in the present work. The spurious particle emission due to incomplete (numerical) Pauli blocking destroys the stability of nuclei on the long time scales of the order of ten periods of GMR oscillations and has been subtracted. This, however, produce a systematic error of about 30% in our results on the GMR damping width.

Overall, the full BUU calculation underestimates the total GMR width by about 30–50%. This might be related to the missed Landau damping contribution in our semiclassical approach, as the comparison between Vlasov and RPA calculations may indicate. Moreover, the memory effects in a collision integral neglected in our calculations also increase the widths of giant multipole resonances.

In conclusion, the breathing mode energies and widths in medium-to-heavy nuclei are reasonably well described within the GiBUU approach, when the same Hamiltonian energy functional is consistently used in the initialization procedure of nuclear ground states and their phase-space evolution. Thus, an extension of the present work to investigate other modes of collective excitation, such as isovector dipole and isoscalar quadrupole resonances, seems possible and would be a helpful tool to understand better the dynamics in low energy reaction physics. Future transport applications to fusion/deep-inelastic collisions for isospin asymmetric systems to investigate exotic collective modes in neutron-rich finite systems, such as the pigmy dipole resonance, seem possible. Furthermore, the improved transport model may be a better tool in theoretically describing hadron-induced reactions, in-particular the proton-induced those leading to nuclear fragmentation, and very peripheral heavy-ion collisions, in which the stability of nuclear ground states is essential.

Acknowledgments: We are grateful to I.N. Mishustin, N. Tsoneva for stimulating discussions and their interest in this work, and to M. Kaskulov for his useful suggestions in extracting the width. This work is supported by the Helmholtz International Center for

FAIR within the framework of the LOEWE program and by BMBF.

- [1] M.N. Harakeh and A. van der Woude, *Giant Resonances: Fundamental High-Frequency Modes of Nuclear Excitation*, Oxford Univ. Press, Oxford (2001).
- [2] J.P. Blaizot, Phys. Rep. **64**, 171 (1980).
- [3] I. Hamamoto, H. Sagawa, and H.Z. Zhang, Phys. Rev. C **56**, 3121 (1997).
- [4] H. Sagawa, S. Yoshida, G.M. Zeng, J.Z. Gu, and X.Z. Zhang, Phys. Rev. C **76**, 034327 (2007).
- [5] J. Piekarewicz, Phys. Rev. C **64**, 024307 (2001).
- [6] J. Piekarewicz and M. Centelles, Phys. Rev. C **79**, 054311 (2009).
- [7] Ph. Chomaz, Nguyen Van Giai, and S. Stringari, Phys. Lett. **B189**, 375 (1987).
- [8] D. Vretenar, G.A. Lalazissis, R. Behnsch, W. Pöschl, P. Ring, Nucl. Phys. **A621**, 853 (1997).
- [9] M.V. Stoitsov, M.L. Cescato, P. Ring, M.M. Sharma, J. Phys. G: Nucl. Part. Phys. **20**, L149 (1994).
- [10] M.M. Sharma, Nuc. Phys. A **816**, 65 (2009).
- [11] F.E. Bertrand, Nucl. Phys. **A354**, 129c (1981).
- [12] A. Bonasera, G.F. Burgio and M. Di Toro, Phys. Lett. B **221**, 233 (1989).
- [13] A. Bonasera, M. Di Toro, and F. Gulminelli, Phys. Rev. C **42**, 966 (1990).
- [14] A. Smerzi, A. Bonasera, and M. Di Toro, Phys. Rev. C **44**, 1713 (1991).
- [15] S. Ayik and D. Boilley, Phys. Lett. B **276**, 263 (1992).
- [16] M. Belkacem, S. Ayik, and A. Bonasera, Phys. Rev. C **52**, 2499 (1995).
- [17] V.M. Kolomietz, V.A. Plujko and S. Shlomo, Phys. Rev. C **54**, 3014 (1996).
- [18] V.I. Abrosimov, O.I. Davidovskaja, V.M. Kolomietz, and S. Shlomo, Phys. Rev. C **57**, 2342 (1998).
- [19] M. Di Toro, V.M. Kolomietz, and A.B. Larionov, Phys. Rev. C **59**, 3099 (1999).
- [20] K. Morawetz, U. Fuhrmann, R. Walke, arXiv:nucl-th/0001032v3. Isospin Physics in Heavy-Ion Collisions at Intermediate Energies, Bao-An Li, W. U. Schroeder, ed. ,Nova Science Publishers, New York (2001).
- [21] S. Yildirim, T. Gaitanos, M. Di Toro, V. Greco, Phys. Rev. **C72**, 064317 (2005).
- [22] L.P. Kadanoff, G. Baym, *Quantum Statistical Mechanics* (Benjamin, New York, (1962).
- [23] V. Baran, C. Rizzo, M. Colonna, M. Di Toro, and D. Pierroutsakou, Phys. Rev. C **79**,

- 021603(R) (2009).
- [24] D. Pierroutsakou et al., Phys. Rev. C **80**, 024612 (2009).
 - [25] A.B. Larionov, J. Piperova, M. Colonna, and M. Di Toro, Phys. Rev. C **61**, 064614 (2000).
 - [26] A.B. Larionov, O. Buss, K. Gallmeister, and U. Mosel, Phys. Rev. C **76**, 044909 (2007).
 - [27] A.B. Larionov, I.N. Mishustin, L.M. Satarov, W. Greiner, Phys.Rev. **C78**, 014604 (2008).
 - [28] T. Gaitanos, H. Lenske, and U. Mosel, Phys. Lett. B **663**, 197 (2008).
 - [29] <http://gibuu.physik.uni-giessen.de/GiBUU>.
 - [30] B. Serot and J.D. Walecka, Int. J. Mod. Phys. **E6** (1997) 631.
 - [31] J. Boguta and A.R. Bodmer, Nucl. Phys. A **292**, 413 (1977).
 - [32] G.A. Lalazissis, S. Karatzikos, R. Fossion, D. Pena Arteaga, A.V. Afanasjev, P. Ring, Phys. Lett. **B671**, 36 (2009).
 - [33] G.A. Lalazissis, J. Konig, and P. Ring, Phys. Rev. C **55**, 540 (1997).
 - [34] T. Gaitanos, M. Kaskulov, U. Mosel, Nucl. Phys. **A828**, 9 (2009).
 - [35] B. Blättel, V. Koch, U. Mosel, Rep. Prog. Phys. **56**, 1 (1993).
 - [36] A. Andronic (FOPI Collaboration), Phys. Lett. **B612**, 173 (2005), and references therein.
 - [37] V.B. Berestetskii, E.M. Lifschitz, L.P. Pitaevskii, *Quantum Electrodynamics in Russian*, Moscow “Nauka” (1989).
 - [38] O. Buss, PhD thesis, Giessen 2008, <http://gibuu.physik.uni-giessen.de/GiBUU/wiki/Paper>.
 - [39] J. Blocki, Y. Boneh, J.R. Nix, J. Randrup, M. Robel, A.J. Sierk, and W.J. Swiatecki, Ann. Phys. (N.Y.) **113**, 330 (1978).
 - [40] A.J. Sierk, S.E. Koonin, and J.R. Nix, Phys. Rev. C **17**, 646 (1978).
 - [41] J. Piekarewicz, Phys. Rev. C **66**, 034305 (2002).
 - [42] D. Vretenar, T. Nikić, P. Ring, Phys. Rev. C **68**, 024310 (2003).
 - [43] T. Li et al., Phys. Rev. Lett. **99**, 162503 (2007).
 - [44] V. Baran, M. Colonna, V. Greco, and M. Di Toro, Phys. Rep. **410**, 335 (2005).
 - [45] A. Bohr and B. Mottelson, *Nuclear structure*, Vol. 2, Benjamin, New York (1975).
 - [46] A.A. Abrikosov and I.M. Khalatnikov, Rep. Prog. Phys. **22**, 329 (1959).
 - [47] V.M. Kolomietz, A.B. Larionov, M. Di Toro, Nucl. Phys. A **613**, 1 (1997).
 - [48] S. Shlomo, D.H. Youngblood, Phys. Rev. **C47**, 529 (1993).
 - [49] G. Bertsch, Z. Phys. A **289**, 103 (1978).
 - [50] G.A. Brooker and J. Sykes, Ann. Phys. (N.Y.) **61**, 387 (1970).

- [51] A.B. Larionov, M. Cabibbo, V. Baran, M. Di Toro, Nucl. Phys. A **648**, 157 (1999).
- [52] P. Ring, P. Schuck, *The nuclear many-body problem*, Springer Verlag, (1980).
- [53] Ph. Chomaz, GANIL Report P 98 01.
- [54] S. Kamedzhiev, J. Specht, G. Tertychny, Phys. Rep. **393**, 1 (2004).
- [55] V. Tselyaev, S. Krewald, E. Litvinova, J. Specht, arXiv:0912.5328 [nucl-th].
- [56] V.I. Tselyaev, Phys. Rev. C **75**, 024306 (2007).